Reflector-less nanoparticles doped optical fiber biosensor for the detection of proteins: Case thrombin

Marzhan Sypabekova, Arman Aitkulov, Wilfried Blanc, Daniele Tosi

Reflector-less nanoparticles doped optical fiber biosensor for the detection of proteins: Case thrombin

Marzhan Sypabekova [a,b,*], Arman Aitkulov [c], Wilfried Blanc [d], Daniele Tosi [a,c]

[a] National Laboratory Astana, Laboratory of Biosensors and Bioinstruments, 010000, Nur-Sultan, Kazakhstan
[b] Nazarbayev University, School of Medicine, 010000, Nur-Sultan, Kazakhstan
[c] Nazarbayev University, School of Engineering and Digital Sciences, 010000, Nur-Sultan, Kazakhstan
[d] Université Côte d'Azur, INPHYNI–CNRS UMR 7010, Parc Valrose, 06108, Nice, France

ARTICLE INFO

Keywords:
Reflector-less biosensor
Optical fiber biosensor
Evanescent wave biosensor
Biodetection
Rayleigh scattering

ABSTRACT

A miniature biosensing platform based on MgO-based nanoparticle doped optical fiber was developed for the biomolecule detection. The technology used a single mode fiber with MgO-based nanoparticles doped core. The detection was based on collecting the Rayleigh backscattering signatures with increased gain upon the etching of the fiber 1–2 mm away from the tip. The shift from the backscattered signal with the maximum value of the cross-correlation was used to report the results. The sensor exhibited a sensitivity range from 0.75 nm/refractive index unit up to 19.63 nm/refractive index unit for a refractive index range from 1.3329 up to 1.37649. The deposition of the thin gold layer increased the overall sensitivity of the biosensor by 3.7 times for the etched part of the fiber with diameter 8–9 μm. The proposed biosensor was tested for the detection of thrombin molecule concentrations ranging from 0.625 μg/ml to 20 μg/ml. Thiol modified DNA specific aptamers were used to functionalize the gold coated surface of the fiber for the detection. The sensor showed detectable sensitivity and specificity as compared to the other control proteins. The proposed biosensing platform could be multiplexed and can be used *in vivo* for the detection in clinical settings due to its miniature size, biocompatibility of silica glass and reflector less set up.

1. Introduction

In the last decade, biosensors based on optical fibers have drawn an interest due to its attractive characteristics such as compact size, flexibility, relative low cost and biocompatibility (Yin et al., 2018). They also have magnetic resonance compatibility as well as long-range and multiplexed detection capability (Molardi et al., 2019), and therefore have found many applications in different fields (Socorro-Leránoz et al., 2019). Physical characteristics of the optical fibers enables to measure the level of the biomarkers in biological liquids, non-liquid media and in hard to reach environments for minimally-invasive *in vivo* medical diagnosis (Ribaut et al., 2017). Most of the biosensors based on optical fibers used the same principle of operation such as immobilization of the bioreceptors and recognition elements for capturing and label-free detection of the analyte in the form of proteins and cells (Bekmurzayeva et al., 2018; Lao et al., 2019; Loyez et al., 2018; Marzhan Sypabekova et al., 2019). The Refractive index (RI) change around the fiber surface, *i.e.* the biological binding event, is then detected by the light which is propagated within the core of the optical fiber. To enable the detection the structure of the fiber is usually altered at a specific sensing point such a way that the light can escape the core of the fiber and get into contact with the surrounding medium. The change in the surrounding medium provokes the initiation of the altered light spectrum. The altered spectrum of the transmitted or reflected light is then usually detected by the instruments such as optical spectrum or vector analyzer.

Grating-based biosensors are one of the most common type of fiber optic biosensors, thanks to the compact format and a micro-fabrication process, either through a phase mask (Mihailov et al., 2011) or by direct inscription with a femtosecond laser (Martinez et al., 2004). While the fiber Bragg grating (FBG) is not itself suitable for RI sensing, by modifying either the fiber structure (Leung et al., 2007), or the grating profile (Loyez et al., 2018), or both (Marzhan Sypabekova et al., 2019) it is possible to introduce a substantial RI sensitivity. The inscription of the gratings into a fiber encodes the sensing principle in the change of the effective RI of the modes propagating in the fiber, which results in a

* Corresponding author. National Laboratory Astana, Laboratory of Biosensors and Bioinstruments, 010000, Nur-Sultan, Kazakhstan.
E-mail address: msypabekova@nu.edu.kz (M. Sypabekova).

change of the resonant wavelengths that can be interrogated (Leung et al., 2007). The FBGs in this regard can be inscribed in different geometrical configurations (Fig. 1). Several biosensors have been reported which are based on grating inscription, namely etched FBG (Bekmurzayeva et al., 2018), tilted FBG (TFBG) (Lao et al., 2019; Ribaut et al., 2017), etched TFBG (Marzhan Sypabekova et al., 2019) and long period grating (LPG) (Esposito et al., 2018).

Grating based biosensors have proven to be suitable for the biodetection and have shown high sensitivity; however the fabrication of FBGs inside the fiber core at specific region is not easy and not scalable since it requires precise and controlled micro-positioning (Korganbayev et al., 2019). Therefore the possibility of mass production is limited due to the complexity of the fabrication. Moreover, TFBG, LPG and plasmonic devices based on TFBG work in transmission which requires the fabrication of additional gold tip mirrors to back-reflect the transmission spectrum (Ribaut et al., 2017) and also external polarization controllers.

An alternative to reflective gratings that are inscribed within the core of the optical fibers is the development of a grating-free or reflector-less sensor. In the previously described FBG configuration the change of effective RI surrounding the fiber, *i.e.* the biosensing principle, is converted into a change of the FBG reflection spectrum. However, the research on optical backscatter reflectometry (OBR) carried out by Froggatt and Moore (1998) showed that, even in absence of a reflective element such as a grating, Rayleigh scattering acts as the reflective element into the fiber. Since Rayleigh scattering is present in all fibers used in biosensors, we label the OBR-based technique as "reflector-less", to emphasize the lack of a reflective element, replaced by the intrinsic reflection already present in the fiber. Therefore, the fiber optic sensors based on "reflector-less" architecture does not require neither the fabrication of a reflective element or microstructures inside the fiber, nor the detection of optical spectrum serving towards low cost and yet reliable sensing device as compared to grating assisted fiber optic sensors. The detection in "reflector-less" sensors is rather based on processing the information and demodulation of the scattering power traces of backscattering fiber. Such fibers allow the detection of the signal capable of sustaining the evanescent field losses (Korganbayev et al., 2019) at wide range of RI. In addition, "reflector-less" fiber optic devices unlike grating assisted fibers do not require the fabrication of reflective gold mirrors at the tip of the fiber, generation of signal based on surface plasmon resonance, as well as the use of external polarization controllers (Fig. 1) contributing to the cost-effectiveness of the device even further. The main point of the current work is that the sensor does not need any grating, surface plasmon resonance, microcavity, or interferometer but just exploits a property (Rayleigh scattering) that the fiber already has, and a fabrication process (wet-etching) used in large batch in electronics. Wet-etching is commonly performed in etching of photoresist (Iliescu et al., 2005), in electronic patterning (Eidelloth et al., 1991) and in other large-volume fabrication.

A good example of such sensor is the nanoparticle doped fiber which generates the Rayleigh scattering. MgO-based nanoparticle doped fibers have the same typical size of a telecom fiber, with a core diameter of 10 μm and a cladding diameter of 125 μm and with randomly distributed nanoparticles size between 2 and 100 nm (Blanc et al., 2019, 2011; MacChesney et al., 1974). MgO-based nanoparticle doped fibers are made by the established chemical vapor deposition (CVD) technique where the fabrication is simplified and cost effective (Sypabekova et al., 2018). In such sensors the analysis of the results is based on the processed information from the reflection spectrum of the Rayleigh backscattering with an OBR (Korganbayev et al., 2019; Sypabekova et al., 2018). The value proposition of such fibers is that the Rayleigh backscattering have a "gain", *i.e.* they scatter more than a standard fiber. When the fiber is etched, there is enough nanoparticles induced scattering to be detected due to the substantial increase of Rayleigh scattering. Hence, the only fabrication step involved in generation of reflector-less sensors is the chemical wet-etching step (usually with hydrofluoric acid) that is used to reduce the cladding thickness of the fibers such as FBG and TFBG. The wet etching is compatible with high-volume manufacturing and hence it is commonly used in mass production of electronic circuitry (Spierings, 1993). Recent works showed that MgO-based nanoparticle doped fibers can be used as RI sensors, prone for temperature compensation (Korganbayev et al., 2019; Sypabekova et al., 2018), and can also be used in spatial multiplexing for parallel connected several fiber sensors (Ayupova et al., 2019; Molardi et al., 2019).

In this work we investigate further the capabilities of the MgO-based nanoparticle doped reflector-less biosensor by functionalizing the surface of the etched fiber with ssDNA aptamer specific to thrombin molecule. As the binding between the thrombin aptamer and thrombin molecule is well studied and established and has been used in the development of different biosensors we have chosen to detect this interaction on our platform. The MgO-based nanoparticle doped fibers were fabricated as in (Sypabekova et al., 2018). The fiber was first etched with hydrofluoric acid. The deposition of the thin gold (Au) layer using the Au electroless plating method to conjugate thiol modified thrombin aptamers on the pre-treated fiber surface for the following protein detection. The application of the thin Au layer increased the overall sensitivity of the fiber by 3.7 times for the etched part of the fiber with diameter 8–9 μm. The specific binding of the thrombin induced the scattering spectra shift which was detected by the OBR.

		Fabrication of reflective element	Fabrication of gold tip mirrors	Require external polarization controllers	RI detection range	Sensitivity (nm/RIU)	Ref.
Grating based	TFBG 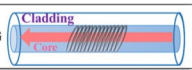	yes	yes	yes	1.3567-1.3592	55	(Cauchet eur et al., 2018)
	etched TFBG 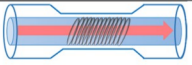	yes	yes	no	1.3418-1.4419	23.38	(Marzhan Sypabekova et al., 2019)
	etched FBG 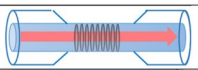	yes	no	no	1.3352-1.4200	17.4	(Bekmurzayeva et al., 2018)
	LPG 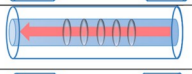	yes	yes	no	1.359–1.419	50	(Chong et al., 2004)
Grating free	MgO doped 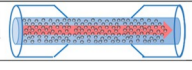	no	no	no	1.3329-1.37649	19.63	This work

Fig. 1. Comparison of fabrication steps and performance of the grating assisted and grating free fiber optic sensors. Schematic representation of the grating based optical fiber biosensors and nanoparticles doped biosensor. The direction of the arrow within the fiber core indicates the working principles based on either (right) reflection or (left) transmission mode (Caucheteur et al., 2018; Chong et al., 2004).

2. Materials and methods

2.1. Reagents

Sulfuric acid (99%, H_2SO_4), Hydrogen Peroxide (30 wt % in H_2O, ACS reagent, H_2O_2), (3-Aminopropyl)trimethoxysilane (97%, APTMS), methanol (for HPLC, ≥99.9%), Au nanoparticles (10 nm diameter, OD 1, AuNP), Gold(III) chloride trihydrate (99.9% trace metals basis, $HAuCl_4$ $3H_2O$), sulfate hydroxylamine (99%, $(NH_2OH)_2$ H_2SO_4), sodium phosphate (BioReagent, Na_2HPO_4), thrombin (from human plasma), phosphate buffered saline (tablet, PBS), 6-Mercapto-1-hexanol (99%, MCH) and DL-Dithiothreitol (BioXtra, ≥99.0%, DTT) were purchased from Sigma-Aldrich. The sequence of the thrombin aptamer was as follow 5′ SH–$(CH_2)_6$–GGTTGGTGTGGTTGG 3' and it was purchased from Sigma Genosis. Sodium Dodecyl Sulfate (white powder, electrophoresis, SDS) was purchased from Fischer Scientific. NAP-5 column (Sephadex G-25 DNA Grade) was purchased from GE Healthcare. All buffers were prepared freshly in diH_2O (18.2 MΩcm) and protein solutions were prepared in 10 mM PBS at pH 7.4.

2.2. Interrogation set up

The experimental set up and interrogation used for the development of the system is shown in Fig. 2. The MgO-based nanoparticles used in this study were formed within the core of the fiber *i.e.* involved in transmission/reflection of the light along the fiber. The MgO-based nanoparticle doped fibers were developed as in (Sypabekova et al., 2018). The key idea is that MgO-based nanoparticles are formed during the fabrication process of the fiber, exactly by a combination of high-temperature and the drawing of the preform, which causes the Mg and O components to cluster into nanoparticles with 20–100 nm diameter (Blanc et al., 2012, 2011). Briefly, the modified CVD method was used to heat the porous substrate of silica doped with a solution of $MgCl_2$ to allow the spontaneous phase separation between silica and the alkaline ion. This separation created two phases: 1) rich with silica and 2) made of MgO-rich spherical particles. The concentration of MgO in each particle varied according to the random process of phase separation (Blanc et al., 2019). Consequently, the size of the particles in the core of the fiber varied and distribution followed a random pattern. This variation was needed to tailor the Rayleigh scattering of the fiber and hence making it possible to detect a change in the spatial operation window of the sensor.

The wavelength shift and the Rayleigh scattered spectra of an MgO-based nanoparticle doped fiber (with attenuation value of 61.5 dB/m) was interrogated using an OBR (Luna OBR4600, Luna Inc., US) with a resolution of 8 p.m., a wavelength window between 1530 and 1616.4 nm and operating in distributed sensing mode at a speed of 3 Hz. The wavelength shift at the etched region with the maximum value of the

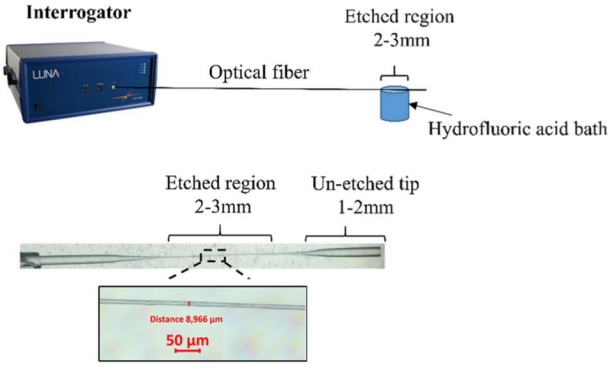

Fig. 2. Schematic view of the experimental set up for etching process. The microscope image shows the dimensions of the etched region of the MgO-based nanoparticle doped fiber.

cross-correlation was chosen to report the results. All measurements were carried out in triplicate, and the mean value of replicates, standard deviations and standard errors from the mean were used to report the results. The interrogator was used for the interrogation of the MgO-based nanoparticle doped fiber spectra throughout calibration, fabrication and functionalization steps, as well as for the detection during thrombin measurements.

2.3. Chemical etching and RI measurement

The output of the OBR was connected to the MgO-based nanoparticle doped fiber (21 cm) through an SMF (single-mode fiber) pigtail. SMF pool was spliced to the MgO-based nanoparticle doped fiber using a standard splicer (Fujikura 12-S, SMF-SMF splicing mode). The tip of the fiber was cut using fiber cleaver (AFL, CT08) and further etched about 1–2 mm away from the tip by immersing the fiber (approx. 2–3 mm) in a solution of 48% hydrofluoric acid (Fig. 2) under the chemical laminar hood (Waldner Secuflow airflow controller, ceiling-bench mounted) at room temperature. Once the difference in Rayleigh scattered spectra or a loss pattern started to appear the etching process was stopped by rinsing the fiber tip thoroughly with diH_2O several times to remove remaining hydrofluoric acid residues. The RI calibration was done by completely immersing the etched tip of the fiber into the sucrose solution with different RI 1.3329; 1.34041; 1.35518; 1.36097; 1.37649. diH_2O was used as a reference during the calibration. The RI of each solution was measured using an automatic digital refractometer (Anton Paar, Inc., Abbemat 300). The wavelength shift was accomplished by running the OBR in distributed sensing mode. The RI calibration of the fibers was done before and after etching, after electroless plating procedure and aptamer immobilization step.

2.4. The deposition of gold on fiber using Au electroless plating method

The electroless plating was conducted as reported in (Loyez et al., 2019b). The etched fiber was cleaned with piranha solution (70% H_2SO_4: 30% H_2O_2) for 10 min. After the fiber was rinsed with diH_2O and immersed in 1% APTMS in methanol for 20 min and rinsed with methanol. The fiber was then dried for 15 min at 80 °C in the oven (Carbolite Gero 30–3000C). The fiber was placed in 10 nm AuNPs solution for 1h at room temperature. The fiber was then washed with diH_2O and immersed in 3 mM $HAuCl_4$ $3H_2O$, 0.4 mM NH_2OH H_2SO_4 for 3 min at room temperature followed by washing with diH_2O.

2.5. The reduction of thiol modified oligonucleotides

The thiol modified oligonucleotides were reduced in 100 mM solution of DTT in 100 mM sodium phosphate buffer (pH 8.5). The thiol modified oligonucleotides were dissolved in 125 µl of the DTT solution and incubated at room temperature for 1 h. Then the sample flowed through the pre-equilibrated NAP-5 column. The column was equilibrated with 10 ml of sodium phosphate buffer (pH 6). The reaction mixture's volume was brought to 500 µl with the sodium phosphate buffer (pH 6) and allowed to enter the gel bed completely by gravity flow. The reduced thiol modified oligonucleotide was eluted with 500 µl of sodium phosphate buffer (pH 6). The concentration of the eluted mixture was measured using the Nanodrop 2000 (Thermo Fischer Scientific). The aliquots of the reduced thiol-modified oligonucleotides were then stored at −20 °C until further use.

2.6. Microscopy imagining

The etched and functionalized optical fiber after the thrombin molecule detection and analysis was analyzed by Scanning Electron Microscope (SEM, JSM-IT200 (LA) and FeSEM Auriga, Crossbeam 540). The diameter of the etched fiber tip was visualized and estimated by ZEISS Axioscope 5. At the end of each step, the fiber was thoroughly

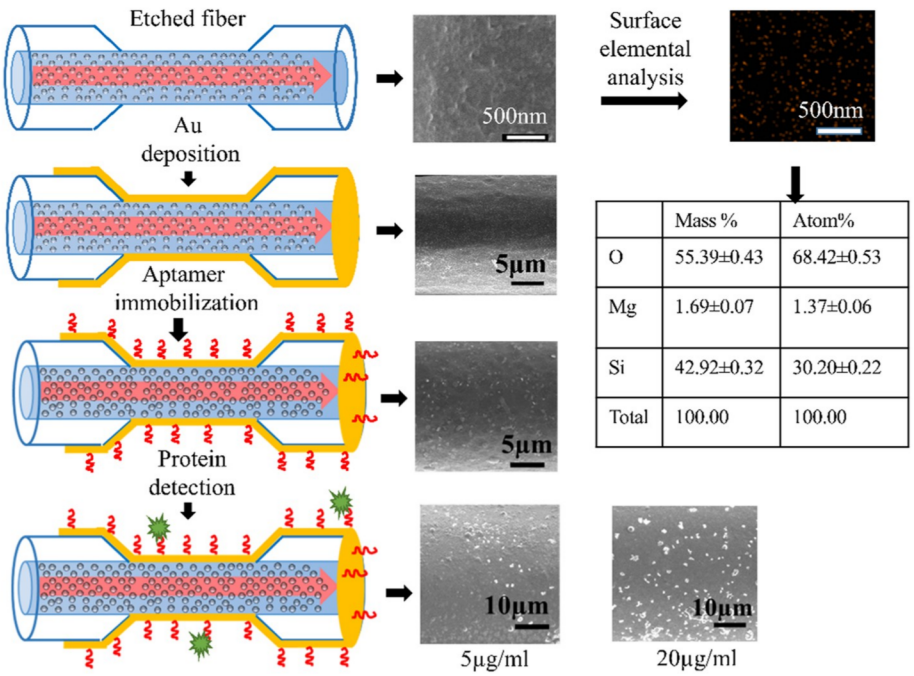

	Mass %	Atom%
O	55.39±0.43	68.42±0.53
Mg	1.69±0.07	1.37±0.06
Si	42.92±0.32	30.20±0.22
Total	100.00	100.00

Fig. 3. Schematic overview of the functionalization of the etched MgO-based nanoparticle doped fiber and thrombin detection. SEM images for an etched, Au deposited, aptamer functionalized fiber and after thrombin detection (5 µg/ml, 20 µg/ml). Surface elemental analysis was conducted by Energy Dispersive X-Ray Spectroscopy on the etched MgO-based nanoparticle doped fiber surface. As the result, Mg (indicated as red dots) and other element traces present in the standard fiber were found on the surface and presented in the table. (For interpretation of the references to colour in this figure legend, the reader is referred to the Web version of this article.)

rinsed with diH_2O (piranha cleaning) and 10 mM PBS (thrombin detection) and allowed to air-dry overnight. 0.5 cm of etched and functionalized optical fiber was then cleaved and glued onto the stubs. For the SEM analysis the samples were gold-sputtered with an automatic sputter coater (Quorum, Q150T) at 3 nm thickness.

2.7. The immobilization of the aptamers and protein detection

3.5 µM thrombin aptamer was diluted in 10 mM PBS buffer and allowed to incubate with the fiber for 16–24 h at −4 °C overnight. The fibers were then rinsed with PBS and backfilled with 1 mM MCH for 1 h at room temperature. The fibers were then rinsed with PBS buffer and allowed to incubate in protein solution for 15 min. After the incubation with the protein the fiber was rinsed by dipping fully and stirring 5 times in a clockwise direction inside the beaker with PBS. Thrombin was diluted in 10 mM PBS at concentrations 20 µg/ml; 5 µg/ml; 2.5 µg/ml; 1.25 µg/ml; 0.625 µg/ml. After the incubation with the protein the fibers were rinsed with PBS buffer and the wavelength shift measurements were conducted in the PBS buffer using an OBR (OBR 4600, Luna Inc.).

2.8. Data analysis

The data acquisition, changes of the wavelength shifts and cross correlation was performed and analyzed through Luna software. The data analysis and statistical analysis was performed with MatLab and focused on the most sensitive point among the spectral shift. The most sensitive point on the tip of the fiber *i.e.* the shifts corresponding to different RI were recorded for several points within the region of interrogation by running the OBR in distributed sensing mode. Baseline variations were compensated for each analysis and the wavelength shifts were then calculated for each tested conditions and for each sensor. During protein measurements PBS was considered as the reference.

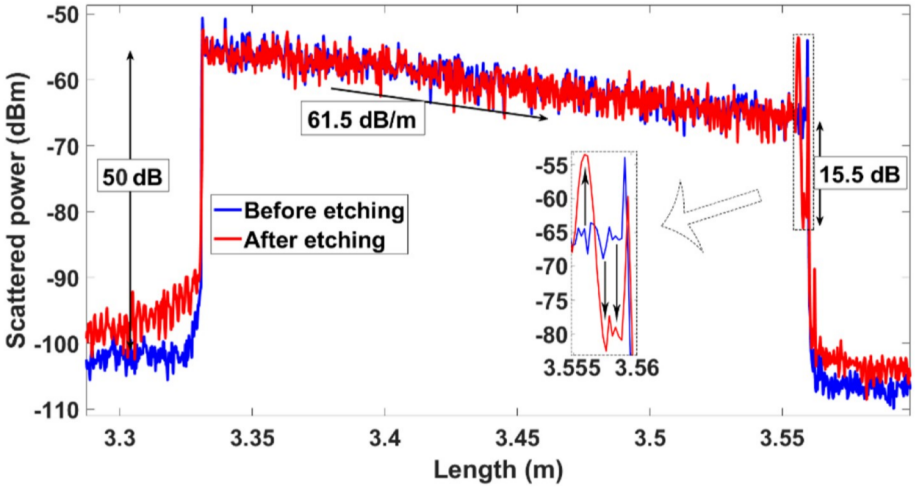

Fig. 4. The typical scattering traces with backscattered power as a function of length of the MgO-based nanoparticle doped fiber before (blue line) and after (red line) etching process. Inset: Scattered spectrum of the un-etched and etched tip. (For interpretation of the references to colour in this figure legend, the reader is referred to the Web version of this article.)

3. Results and discussion

3.1. Etching and the detection of RI

Fig. 4 shows the typical scattering pattern of the MgO-based nanoparticle doped fiber with the backscattered power as a function of the length. It is to be noticed that the MgO-based nanoparticles have the main goal of raising the Rayleigh scattering, so that the signal is detectable with the OBR despite the losses due to the evanescent field in the etched region. The nanoparticle distribution is overall homogeneous, despite the random nature or the deposition, when looking at the millimeter-scale resolution of the OBR. This can be inferred from Fig. 4: the power backscattered by the MgO- based nanoparticle doped fiber has a constant attenuation 61.5 dB/m; the noise is simply the OBR noise, and in fact it occurs also outside of the fiber. Non-homogeneous nanoparticle would mean that the fiber attenuation would be non-constant, which would result in a non-flat descent from 3.35 to 3.5 m in Fig. 4.

According to Fig. 4 the connected SMF with a length of 3.33 m shows the average backscattered power as −98 dBm. After the connection of the MgO-based nanoparticle doped fiber to the SMF we observe a sharp increase in the backscattered power up to −52.4 dBm which corresponds to a "gain" of 50 dB. The gain is an indicative factor showing the difference in scattering trace between the MgO-based nanoparticle doped fiber and standard SMF. The signal from the gain reduces over the length of the MgO-based nanoparticle doped fiber (21 cm) *i.e.* attenuates by 61.5 dB/m due to the loss of the forward and back reflected light. After the etching 1–2 mm away from the tip the scattered power decreases by 15.5 dB (reduced confinement factor) since the diameter of the fiber, which is doped with MgO-based nanoparticles, becomes thinner. The inset of Fig. 4 shows the difference in scattered spectrum between the un-etched and etched tip. The arrows indicate the regions of interrogation at which the sensitivities were analyzed. Prior to the etching the

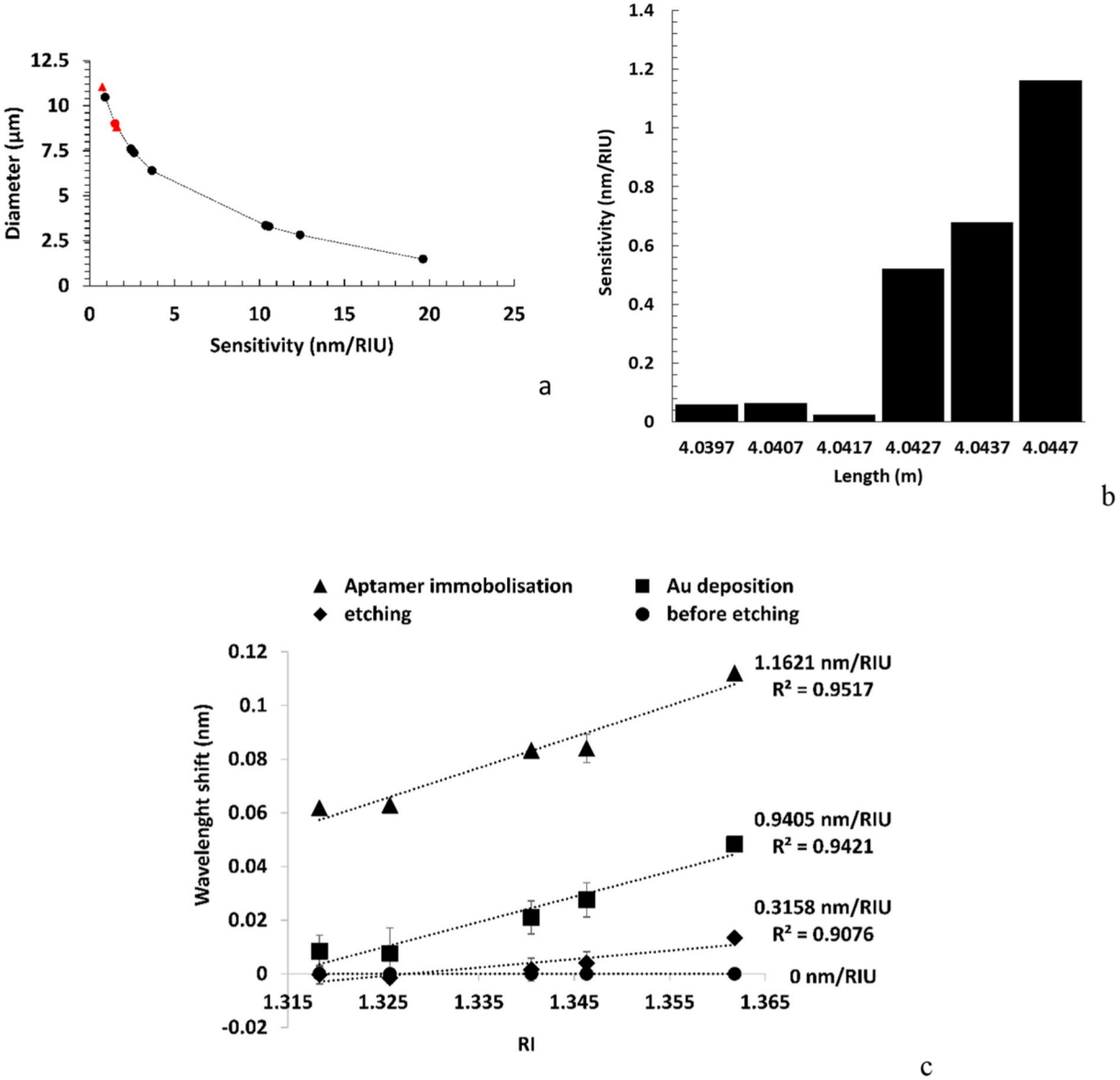

Fig. 5. (a) The relationship between the fiber diameters at etched region versus the fiber sensitivity. Values indicated in red (triangle) represents the measured diameters (using the microscope ZEISS Axioscope 5), values indicated in black (dots) represents the estimated diameters (obtained using the formula: $sensitivity[nm/RIU] = 32.6357 \times e^{-0.3414 \times diameter[\mu m]}$) (b) Sensitivity of the fiber at different points along the length of the etched region, * shows point at which the highest sensitivity was observed (c) Wavelength shift of the Rayleigh scattering signature as a function of the RI change before and after etching process and after the functionalization: Au deposition and aptamer immobilization. Error bars show the mean and spread for three measurements. (For interpretation of the references to colour in this figure legend, the reader is referred to the Web version of this article.)

MgO-based nanoparticles doped fiber did not show any specificity towards the surrounding RI change (Fig. 5c). The specificity started to appear after the etching process took place, where the cladding and part of the core of the fiber was depleted. The sensitivity is calculated by analyzing the changes in wavelength shift showing the maximum value of the cross correlation at the region of interrogation. With an increasing etching time the fiber diameter decreased and hence the sensitivity increased accordingly. The diameter of the several etched fibers was measured using the Axioscope Microscope (Fig. 5a, values indicated in red triangle) and the corresponding sensitivity was measured by immersing the etched tip in solutions with various RI. Since the etching process makes the fiber fragile and hence difficult to place on a microscope slide the diameters for the other etched fibers were estimated using the formula below (values indicated in black dots):

$$Sensitivity[nm/RIU] = 32.6357 \times e^{-0.3414 \times diameter[\mu m]}$$

The curve simulation was performed by adapting the coupled mode theory to thin-cladding FBGs, as in (Iadicicco et al., 2004) (See Supplementary Information Fig. S1). The sensitivity for an etched MgO-based nanoparticle doped fiber was in the range between 0.75 and 19.63 nm/RIU (refractive index unit) and the corresponding diameters were 11.04–1.84 μm. The data indicated that the etching indeed reaches the core of the fiber where the MgO-based nanoparticles are located and hence facilitated the decrease in scattered power. As the fiber diameter gets thinner further manipulations during the functionalization with the fiber becomes difficult unless other automated process or an enclosed chamber is used to reduce the fiber breaking due to the human factor. For this reason within the scope of this work, for the following functionalization we used etched fiber with the diameter in the range of 8–9 μm.

A shift of the backscattered signal was observed when the etched fiber was immersed in sucrose solution due to the change in surrounding RI. This shift was detected by the OBR where the region around a specific point on the reference spectrum (spectrum measured in diH_2O) in length domain was chosen. This particular region was then converted to frequency domain and reinterpreted by cross-correlating the resulting signal. The shift that exhibits the maximum value of the cross-correlation was taken as the main one in presenting the results. In this work the significant difference in wavelength shift of the backscattered signal was at location 4.0447 m (Fig. 5b, **highlighted with asterisk**). Hence, measurements at point 4.0447 m were used for the analysis of the data during the protein measurements. The etched MgO-based nanoparticle doped fiber was calibrated also in between the functionalization steps, namely after the Au deposition and after the aptamer immobilization. This was measured by placing the Au coated fiber in a solution of sucrose with varying RI and consequent result interrogation. The trend of significant increase in sensitivity was observed after the Au deposition from 0.3158 for etched fiber up to 0.9405 nm/RIU for Au coated fiber indicating the importance and influence of the thin Au layer on the fiber sensitivity. The sensitivity of the fiber only slightly increased after the aptamer immobilization by 1.1621 nm/RIU in this particular case (Fig. 5c). The similar trend was observed in all of the fibers we studied where the influence of the Au deposition on the sensitivity was high and the influence of the aptamer immobilization was low or negligible in some cases.

As opposed to temperature variations, it was found that all the fibers (etched and not) were temperature-sensitive with same coefficient of 11.9 p.m./K (Beisenova et al., 2019) where the observed wavelength shift was corrected in the RI-sensing region with the data observed in the temperature-insensitive part which verifies that the temperature variations do not affect the performance of the fiber.

3.2. Thrombin detection

In order to show the potential application of the MgO-based nanoparticle doped etched fiber as opposed to the device and application the biosensing test was further conducted by immobilizing the aptamer on the surface as a bioreceptor and consequent detection of the thrombin molecule as a target. Thrombin is small molecule associated with the blood coagulation process and it is involved in atherosclerosis, thromboembolic, inflammatory disease and cancer disease (Falanga and Marchetti, 2018; Li et al., 2016). Aptamers are synthetic bioreceptors that are being specifically selected against a certain target and they exhibit significant binding capability as well as therapeutic abilities in certain diseases (Li et al., 1994). In this work 15 nucleotide thrombin aptamer selected by (Bock et al., 1992) with a disassociation constant at 25–200 nM range was used. This aptamer has high affinity and specificity towards the thrombin molecule and it had being used in developing different sensors.

The thiol modified aptamer was immobilized on the fiber surface which was coated with Au (Fig. 3). The direct and cost-effective method electroless plating was used to deposit the approximately 35 nm of Au on the etched fiber surface instead of using traditional Au sputtering which requires special facilities. Au usually do not attach well to optical fibers as they are made of silica glass substrate. The attachment could be achieved via molecular linking process such as silanisation. Silanisation is the coupling agent used in the functionalization of optical fiber based biosensors. Therefore the surface of the fiber was first activated with silane coupling agent APTMS followed by the adsorption of Au nanoparticles. Then the fiber was immersed into the plating solution containing the metal ions (Au^{3+}) and the reducing agent (hydroxylamine) at the same time. The Au deposition occurs only when the electronic transfer from the reducer to the metal is slow. Otherwise, all the metal would be reduced into the plating solution and forming black precipitates (Loyez et al., 2019b). The SEM image after the Au deposition is shown in Fig. 3. The morphology of the etched fiber surface under the SEM showed some irregularities and the elemental surface chemistry analysis confirmed the presence of the Mg ions (red dots on SEM image) within the fiber core as 1.69% of the total mass (Fig. 3). The elemental analysis also showed the presence of other elements from which the standard glass optical fiber is made of such as Si (43%) and O (56%).

The estimated aptamer density on gold coated optical fiber surface was 32.2×10^6 pg/mm^2 and it was identified using the formula (Boufffartigues et al., 2007) without taking into consideration the variation of wavelength per unit of variation of refractive index calibrated for the apparatus (OBR in this case):

$$DNA\ density = \frac{\Delta\lambda^* d_b}{\frac{\delta n}{\delta C}}$$

Where, $\delta n/\delta C$ is the dependence of the variation in biological medium refractive index as a function of concentration (for nucleic acids: 1.9×10^{-10} mm^3/pg); d_b the penetration depth of the sensing region in the medium immediately above the gold layer: 1.02×10^{-4} mm; and $\Delta\lambda$ is the variation of wavelength change (expressed as %). It is possible that the aptamer/MCH variation used in this study is not optimal and the uniformity of the surface could vary. However according to SEM images in Fig. 3 and the error bars presented in Fig. 6 showed that the protein detection was possible at different concentrations and the process was repeatable.

Different thrombin concentrations (0.625, 1.125, 2.5, 5 and 20 μg/ml) were incubated with the functionalized fiber and the corresponding spectral signatures were analyzed (see Supplementary Information Fig. S2). After the thrombin incubation the fiber was rinsed with the PBS solution in order to leave only the stable interaction on the surface. The measurement in PBS but without the protein was considered as a reference and subsequently subtracted from all the protein measurements. The lowest concentration 0.625 μg/ml thrombin exhibited the negative wavelength shift (−0.02 nm) after the incubation. Once the concentration of the thrombin was increased the wavelength shift increased from 0.02 nm at 1.125 μg/ml up to 0.03 nm at 5 μg/ml (Fig. 6).

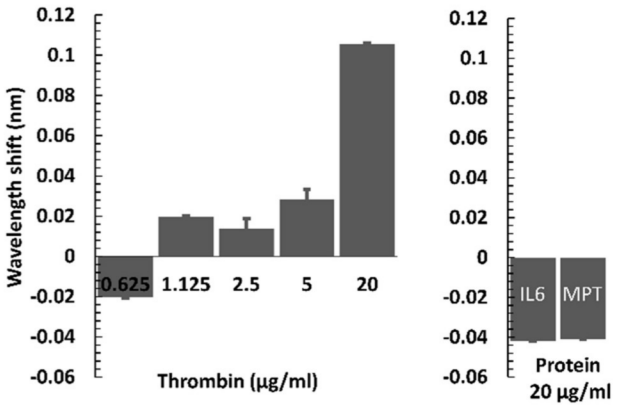

Fig. 6. Analysis of the response of the etched MgO-based nanoparticle doped fiber to thrombin. Wavelength shift observed for thrombin concentrations 0.625, 1.125, 2.5, 20 µg/ml and for the control proteins at 20 µg/ml.

The highest concentration of the thrombin tested was 20 µg/ml which exhibited the increase in wavelength shift up to 0.11 nm. According to the SEM analysis after the incubation with the thrombin (5 µg/ml) molecule the surface of the fiber contained spherical shaped dots. The number of spherical shapes were increased when the fiber was incubated with 20 µg/ml thrombin molecule. More analytical methods such as secondary fluorescent antibody application and visualization need to be carried out to confirm that the increased number of dots indeed correspond to thrombin protein. To better justify the foundation of the selection, we have used two control proteins namely MPT64 and IL6. Both control proteins in other works showed some degree of affinity to different aptamer sequences (Gupta et al., 2014; Sypabekova et al., 2018a). Il-6 is cytokine which is secreted by various types of cells including tumor cells. It is involved in proliferation and differentiation of the malignant cells (Kumari et al., 2016). MPT (64) is secreted protein by the bacterium associated with the Tuberculosis disease ((Bekmurzayeva et al., 2013). Noteworthy, two control proteins IL-6 and MPT (64) at 20 µg/ml provided a negative shift as compared to the thrombin at concentrations above 0.625 µg/ml (Fig. 6). The negative values in wavelength shift for the control proteins and for the thrombin at 0.6255 µg/ml concentration could be due to different RI formed at the surface of the fiber as compared to thrombin concentrations between 1.125 and 20 µg/ml. The wavelength shift obtained with controls was similar to the wavelength shift at analyte concentration well below limit of detection. Both thrombin and control proteins were diluted in PBS and incubation was conducted at room temperature. The error bars describing the uncertainty of the method show the mean and spread for at least three measurements. The surface chemistry used in this study was based on simple procedure where thiol modified aptamers were immobilized overnight on an Au coated fiber surface and backfilled with the MCH. Bare gold surface is known to be sticky to proteins and also to DNA (Li et al., 2010; Sandström et al., 2003). To avoid the non-specific binding to the bare gold surface, co-adsorbent molecules can be used (Jolly et al., 2015; Miodek et al., 2015; Nogues et al., 2012). In addition, such molecules are also needed to align well the DNA layer on the surface (Bai et al., 2013). Backfilling with MCH at1mM concentration was used to uniformly cover the surface after aptamer attachment and hence to eliminate the non-specific adsorption of proteins to the Au surface to some extent (Bai et al., 2013; Jolly et al., 2017; Miodek et al., 2015; M. Sypabekova et al., 2019). Previous studies those related to the thrombin sensing using optical fibers involved the use of grating assisted optical fibers such as FBG's (Bekmurzayeva et al., 2018), TFBG's (Albert et al., 2013; Lao et al., 2019; Shevchenko et al., 2011; Marzhan Sypabekova et al., 2019) and LPG's (Coelho et al., 2016). Such fibers require complex fabrication steps where the gratings need to be inscribed in the fiber, using a phase mask or femtosecond laser inscription method. In addition LPG and TFBG based sensors work in transmission mode which means that a reflecting element such as golden mirror needs to be fabricated to back reflect the transmission. The current work bypasses both grating inscription and fabrication of the reflecting element. The recent work on thrombin biosensors include plasmonic (Kotlarek et al., 2019), electrochemiluminescence (Isildak et al., 2020), capacitive (Chen et al., 2019), piezoelectric (Bayramoglu et al., 2019), lateral flow assay (Gao et al., 2019) and electrochemical (Hu et al., 2020). Each of these sensors have different mode of operation as well as different surface chemistry and signal amplification strategies. As compared to above biosensor types optical fiber based biosensors have significant advantages including cost-effectiveness, small size, flexibility, light weight, remote detection capability, magnetic resonance compatibility (Yin et al., 2018), minimally invasiveness as well immediate detection in non-liquid media such as human tissues (Loyez et al., 2019a; Ribaut et al., 2017). The physical characteristics of the optical fiber allow to be inserted inside the needle or a catheter, to be designed as hand-held probe for in situ measurements. More interestingly the signal from fiber optic sensors is stable and accurate and does not require sophisticated signal processing unit. Thrombin biomolecule measurements clearly shows that the detection using the etched MgO-based nanoparticle doped fiber is possible and hence could serve as a platform for the detection of other biomolecules and biomarkers. It should also be noted that more kinds of proteins could be tested to demonstrate further the selectivity of the developed sensor based on fiber optic device. It should be also noted that the surface chemistry used in this study was not the best as opposed to the surface chemistry published in regards to electrochemical thrombin sensors. This work rather showed the applicability of the reflector-less set up compared to grating assisted fiber optic sensors for the detection of RI change and target protein using the simplest surface chemistry. Therefore, the better and optimized aptamer immobilization strategy needs to be taken into account in the future while using this platform for the certain type and specific target detection.

4. Conclusion

In this work we present the application and use of the etched MgO-based nanoparticle doped reflector-less biosensor for label free detection of the protein. This work is based on sensing the surrounding RI change by optimizing the fiber structure through wet-chemical etching with hydrofluoric acid. The etching was used to deplete the cladding of the fiber and also part of the core which allowed to monitor the Rayleigh scattering effect. The highest sensitivity reached during this work was 19.63 nm/RIU which is 13 times higher from the previously published work (Sypabekova et al., 2018). With an appropriate engineering the development of biosensors using the etched MgO fiber is possible and could be developed further. In this work, we used an etched MgO fiber for the detection of thrombin molecule. Molecular recognition scheme based on thrombin aptamer immobilization on the Au film showed a reasonable sensitivity towards the thrombin and relatively good specificity as compared to other proteins tested providing its potential for biomarker detection. Moreover the current work also shows that the sensitivity of the sensor improves after the deposition of the gold layer as compared to etched fiber. The proposed work is a minimalistic and scalable version of a fiber optic biosensor, which is based only on etching a fiber in hydrofluoric acid, a process well established in industrial electronics and photolithography; the fiber used in this experiments can be spooled and spliced like any telecommunication fiber, making this configuration attractive in terms of cost of manufacturing and scalability. Future work will revolve on optimizing the nanoparticle density and distribution to increase the sensitivity. Moreover, surface chemistry optimization studies including the aptamer linker and co-adsorbent type, aptamer/co-adsorbent ratio, testing to more than two control proteins and validating the sensor performance in clinical samples could be investigated in detail.

Funding sources

The research was funded by Nazarbayev University, under grants SMARTER (core: 091019CRP2117) and EPICGuide (code: 240919FD3908). This work was partly supported by ANR Project NanoSlim (ANR-17-CE08-0002).

Declaration of competing interest

The authors declare that they have no known competing financial interests or personal relationships that could have appeared to influence the work reported in this paper.

CRediT authorship contribution statement

Marzhan Sypabekova: Conceptualization, Methodology, Investigation, Formal analysis, Validation, Visualization, Writing - original draft. **Arman Aitkulov:** Software, Data curation, Formal analysis. **Wilfried Blanc:** Investigation, Methodology, Writing - review & editing. **Daniele Tosi:** Conceptualization, Formal analysis, Supervision, Writing - review & editing, Funding acquisition.

Acknowledgement

We would like to acknowledge the members of the Core Facility at Nazarbayev University for their help in conducting SEM imaging. We thank M. Ude and S. Trzesien for the fabrication of the preform and the fiber.

Appendix A. Supplementary data

Supplementary data to this article can be found online at https://doi.org/10.1016/j.bios.2020.112365.

References

Albert, J., Shao, L.-Y., Caucheteur, C., 2013. Tilted fiber Bragg grating sensors. Laser Photon. Rev. 7, 83–108. https://doi.org/10.1002/lpor.201100039.

Ayupova, T., Tosi, D., Shaimerdenova, M., Korganbayev, S., Sypabekova, M., Bekmurzayeva, A., Blanc, W., Sales, S., Guo, T., Molardi, C., 2019. Fiber optic refractive index distributed multi-sensors by scattering-level multiplexing with MgO nanoparticle-doped fibers. IEEE Sensor. J. 1–1 https://doi.org/10.1109/JSEN.2019.2953231.

Bai, H.-Y., Campo, F.J. Del, Tsai, Y.-C., 2013. Sensitive electrochemical thrombin aptasensor based on gold disk microelectrode arrays. Biosens. Bioelectron. 42, 17–22. https://doi.org/10.1016/j.bios.2012.10.063.

Bayramoglu, G., Ozalp, C., Oztekin, M., Guler, U., Salih, B., Arica, M.Y., 2019. Design of an aptamer-based magnetic adsorbent and biosensor systems for selective and sensitive separation and detection of thrombin. Talanta. https://doi.org/10.1016/j.talanta.2018.08.048.

Beisenova, A., Issatayeva, A., Sovetov, S., Korganbayev, S., Jelbuldina, M., Ashikbayeva, Z., Blanc, W., Schena, E., Sales, S., Molardi, C., Tosi, D., 2019. Multi-fiber distributed thermal profiling of minimally invasive thermal ablation with scattering-level multiplexing in MgO-doped fibers. Biomed. Optic Express 10, 1282. https://doi.org/10.1364/boe.10.001282.

Bekmurzayeva, A., Dukenbayev, K., Shaimerdenova, M., Bekniyazov, I., Ayupova, T., Sypabekova, M., Molardi, C., Tosi, D., 2018. Etched fiber Bragg grating biosensor functionalized with aptamers for detection of thrombin. Sensors 18, 4298. https://doi.org/10.3390/s18124298.

Bekmurzayeva, A., Sypabekova, M., Kanayeva, D., 2013. Tuberculosis diagnosis using immunodominant, secreted antigens of. Mycobacterium tuberculosis. Tuberculosis 93. https://doi.org/10.1016/j.tube.2013.03.003.

Blanc, W., Guillermier, C., Dussardier, B., 2012. Composition of nanoparticles in optical fibers by secondary ion mass spectrometry. Opt. Mater. Express. https://doi.org/10.1364/ome.2.001504.

Blanc, W., Martin, I., Francois-Saint-Cyr, H., Bidault, X., Chaussedent, S., Hombourger, C., Lacomme, S., Le Coustumer, P., Neuville, D.R., Larson, D.J., Prosa, T.J., Guillermier, C., 2019. Compositional changes at the early stages of nanoparticles growth in glasses. J. Phys. Chem. C. https://doi.org/10.1021/acs.jpcc.9b08577.

Blanc, W., Mauroy, V., Nguyen, L., Shivakiran Bhaktha, B.N., Sebbah, P., Pal, B.P., Dussardier, B., 2011. Fabrication of rare earth-doped transparent glass ceramic optical fibers by modified chemical vapor deposition. J. Am. Ceram. Soc. https://doi.org/10.1111/j.1551-2916.2011.04672.x.

Bock, L.C., Griffin, L.C., Latham, J.A., Vermaas, E.H., Toole, J.J., 1992. Selection of single-stranded DNA molecules that bind and inhibit human thrombin. Nature. https://doi.org/10.1038/355564a0.

Bouffartigues, E., Leh, H., Anger-Leroy, M., Rimsky, S., Buckle, M., 2007. Rapid coupling of Surface Plasmon Resonance (SPR and SPRi) and ProteinChip™ based mass spectrometry for the identification of proteins in nucleoprotein interactions. Nucleic Acids Res. https://doi.org/10.1093/nar/gkm030.

Caucheteur, C., Loyez, M., González-Vila, Á., Wattiez, R., 2018. Evaluation of gold layer configuration for plasmonic fiber grating biosensors. Optic Express 26, 24154–24163. https://doi.org/10.1364/OE.26.024154.

Chen, H.J., Chen, R.L.C., Hsieh, B.C., Hsiao, H.Y., Kung, Y., Hou, Y. Te, Cheng, T.J., 2019. Label-free and reagentless capacitive aptasensor for thrombin. Biosens. Bioelectron. https://doi.org/10.1016/j.bios.2019.02.025.

Chong, J.H., Shum, P., Haryono, H., Yohana, A., Rao, M.K., Lu, C., Zhu, Y., 2004. Measurements of refractive index sensitivity using long-period grating refractometer. Optic Commun. https://doi.org/10.1016/j.optcom.2003.10.044.

Coelho, L., de Almeida, J.M.M.M., Santos, J.L., da Silva Jorge, P.A., Martins, M.C.L., Viegas, D., Queirós, R.B., 2016. Aptamer-based fiber sensor for thrombin detection. J. Biomed. Optic. 21, 87005. https://doi.org/10.1117/1.JBO.21.8.087005.

Eidelloth, W., Gallagher, W.J., Robertazzi, R.P., Koch, R.H., Oh, B., Sandstrom, R.L., 1991. Wet etch process for patterning insulators suitable for epitaxial high Tc superconducting thin film multilevel electronic circuits. Appl. Phys. Lett. 59, 1257–1259. https://doi.org/10.1063/1.105469.

Esposito, F., Sansone, L., Taddei, C., Campopiano, S., Giordano, M., Iadicicco, A., 2018. Ultrasensitive biosensor based on long period grating coated with polycarbonate-graphene oxide multilayer. Sensor. Actuator. B Chem. https://doi.org/10.1016/j.snb.2018.08.002.

Falanga, A., Marchetti, M., 2018. Hemostatic biomarkers in cancer progression. Thromb. Res. 164, S54–S61. https://doi.org/10.1016/j.thromres.2018.01.017.

Froggatt, M., Moore, J., 1998. High-spatial-resolution distributed strain measurement in optical fiber with Rayleigh scatter. Appl. Optic. https://doi.org/10.1364/AO.37.001735.

Gao, Y., Zhu, Z., Xi, X., Cao, T., Wen, W., Zhang, X., Wang, S., 2019. An aptamer-based hook-effect-recognizable three-line lateral flow biosensor for rapid detection of thrombin. Biosens. Bioelectron. https://doi.org/10.1016/j.bios.2019.03.036.

Gupta, S., Hirota, M., Waugh, S.M., Murakami, I., Suzuki, T., Muraguchi, M., Shibamori, M., Ishikawa, Y., Jarvis, T.C., Carter, J.D., Zhang, C., Gawande, B., Vrkljan, M., Janjic, N., Schneider, D.J., 2014. Chemically modified DNA aptamers bind interleukin-6 with high affinity and inhibit signaling by blocking its interaction with interleukin-6 receptor. J. Biol. Chem. https://doi.org/10.1074/jbc.M113.532580.

Hu, Q., Bao, Y., Gan, S., Zhang, Y., Han, D., Niu, L., 2020. Amplified electrochemical biosensing of thrombin activity by RAFT polymerization. Anal. Chem. https://doi.org/10.1021/acs.analchem.9b05647.

Iadicicco, A., Cusano, A., Cutolo, A., Bernini, R., Giordano, M., 2004. Thinned fiber Bragg gratings as high sensitivity refractive index sensor. IEEE Photon. Technol. Lett. 16, 1149–1151. https://doi.org/10.1109/LPT.2004.824972.

Iliescu, C., Jing, J., Tay, F.E.H., Miao, J., Sun, T., 2005. Characterization of masking layers for deep wet etching of glass in an improved HF/HCl solution. Surf. Coating. Technol. 198, 314–318. https://doi.org/10.1016/j.surfcoat.2004.10.094.

Isildak, I., Navaeipour, F., Afsharan, H., Kanberoglu, G.S., Agir, I., Ozer, T., Annabi, N., Totu, E.E., Khalilzadeh, B., 2020. Electrochemiluminescence methods using CdS quantum dots in aptamer-based thrombin biosensors: a comparative study. Microchim. Acta. https://doi.org/10.1007/s00604-019-3882-y.

Jolly, P., Formisano, N., Tkáč, J., Kasák, P., Frost, C.G., Estrela, P., 2015. Label-free impedimetric aptasensor with antifouling surface chemistry: a prostate specific antigen case study. Sensor. Actuator. B Chem. 209, 306–312. https://doi.org/10.1016/j.snb.2014.11.083.

Jolly, P., Zhurauski, P., Hammond, J.L., Miodek, A., Liébana, S., Bertok, T., Tkáč, J., Estrela, P., 2017. Self-assembled gold nanoparticles for impedimetric and amperometric detection of a prostate cancer biomarker. Sensor. Actuator. B Chem. 251, 637–643. https://doi.org/10.1016/j.snb.2017.05.040.

Korganbayev, S., Shaimerdenova, M., Ayupova, T., Sypabekova, M., Bekmurzayeva, A., Blanc, W., Molardi, C., Tosi, D., 2019. Refractive index sensor by interrogation of etched MgO nanoparticle-doped optical fiber signature. IEEE Photon. Technol. Lett. https://doi.org/10.1109/LPT.2019.2924652.

Kotlarek, D., Vorobii, M., Ogieglo, W., Knoll, W., Rodriguez-Emmenegger, C., Dostálek, J., 2019. Compact grating-coupled biosensor for the analysis of thrombin. ACS Sens. https://doi.org/10.1021/acssensors.9b00827.

Kumari, N., Dwarakanath, B.S., Das, A., Bhatt, A.N., 2016. Role of interleukin-6 in cancer progression and therapeutic resistance. Tumor Biol. https://doi.org/10.1007/s13277-016-5098-7.

Lao, J., Han, L., Wu, Z., Zhang, X., Huang, Y., Tang, Y., Guo, T., 2019. Gold nanoparticle-functionalized surface plasmon resonance optical fiber biosensor: in situ detection of thrombin with 1 n·M detection limit. J. Lightwave Technol. 37, 2748–2755. https://doi.org/10.1109/JLT.2018.2822827.

Leung, A., Shankar, P.M., Mutharasan, R., 2007. A review of fiber-optic biosensors. Sensor. Actuator. B Chem. 125, 688–703. https://doi.org/10.1016/j.snb.2007.03.010.

Li, L., Zhao, H., Chen, Z., Mu, X., Guo, L., 2010. Aptamer-based electrochemical approach to the detection of thrombin by modification of gold nanoparticles. Anal. Bioanal. Chem. 398, 563–570. https://doi.org/10.1007/s00216-010-3922-2.

Li, S., Zhang, D., Zhang, Q., Lu, Y., Li, N., Chen, Q., Liu, Q., 2016. Electrophoresis-enhanced localized surface plasmon resonance sensing based on nanocup array for thrombin detection. Sensor. Actuator. B Chem. 232, 219–225. https://doi.org/10.1016/j.snb.2016.03.134.

Li, W.X., Kaplan, A.V., Grant, G.W., Toole, J.J., Leung, L.L.K., 1994. A novel nucleotide-based thrombin inhibitor inhibits clot-bound thrombin and reduces arterial platelet thrombus formation. Blood. https://doi.org/10.1182/blood.v83.3.677.bloodjournal833677.

Loyez, M., Albert, J., Caucheteur, C., Wattiez, R., 2018. Cytokeratins biosensing using tilted fiber gratings. Biosensors 8, 74. https://doi.org/10.3390/bios8030074.

Loyez, M., Larrieu, J.-C., Chevineau, S., Remmelink, M., Leduc, D., Bondue, B., Lambert, P., Devière, J., Wattiez, R., Caucheteur, C., 2019a. In situ cancer diagnosis through online plasmonics. Biosens. Bioelectron. 131, 104–112. https://doi.org/10.1016/j.bios.2019.01.062.

Loyez, M., Ribaut, C., Caucheteur, C., Wattiez, R., 2019b. Functionalized gold electroless-plated optical fiber gratings for reliable surface biosensing. Sensor. Actuator. B Chem. 280, 54–61. https://doi.org/10.1016/j.snb.2018.09.115.

MacChesney, J.B., O'connor, P.B., Presby, H.M., 1974. A new technique for the preparation of low-loss and graded-index optical fibers. Proc. IEEE. https://doi.org/10.1109/PROC.1974.9608.

Martinez, A., Dubov, M., Khrushchev, I., Bennion, I., 2004. Direct writing of fibre Bragg gratings by femtosecond laser. Electron. Lett. https://doi.org/10.1049/el:20046050.

Mihailov, S.J., Grobnic, D., Smelser, C.W., Lu, P., Walker, R.B., Ding, H., 2011. Bragg grating inscription in various optical fibers with femtosecond infrared lasers and a phase mask. Opt. Mater. Express. https://doi.org/10.1364/ome.1.000754.

Miodek, A., Regan, E.M., Bhalla, N., Hopkins, N.A., Goodchild, S.A., Estrela, P., 2015. Optimisation and characterisation of anti-fouling ternary SAM layers for impedance-based aptasensors. Sensors 15, 25015–25032. https://doi.org/10.3390/s151025015.

Molardi, C., Beisenova, A., Issatayeva, A., Korganbayev, S., Tosi, D., Blanc, W., 2019. Parallel multiplexing in optical backscatter reflectometry by the use of nano-particles doped optical fiber. https://doi.org/10.1117/12.2510100.

Nogues, C., Leh, H., Lautru, J., Delelis, O., Buckle, M., 2012. Efficient antifouling surface for quantitative surface plasmon resonance based biosensor analysis. PloS One 7, e44287. https://doi.org/10.1371/journal.pone.0044287.

Ribaut, C., Loyez, M., Larrieu, J.-C., Chevineau, S., Lambert, P., Remmelink, M., Wattiez, R., Caucheteur, C., 2017. Cancer biomarker sensing using packaged plasmonic optical fiber gratings: towards in vivo diagnosis. Biosens. Bioelectron. 92, 449–456. https://doi.org/10.1016/j.bios.2016.10.081.

Sandström, P., Boncheva, M., Åkerman, B., 2003. Nonspecific and thiol-specific binding of DNA to gold nanoparticles. Langmuir 19, 7537–7543. https://doi.org/10.1021/la034348u.

Shevchenko, Y., Francis, T.J., Blair, D.A.D., Walsh, R., DeRosa, M.C., Albert, J., 2011. In situ biosensing with a surface plasmon resonance fiber grating aptasensor. Anal. Chem. 83, 7027–7034. https://doi.org/10.1021/ac201641n.

Socorro-Leránoz, A.B., Santano, D., Del Villar, I., Matias, I.R., 2019. Trends in the design of wavelength-based optical fibre biosensors (2008–2018). Biosens. Bioelectron. X 1, 100015. https://doi.org/10.1016/j.biosx.2019.100015.

Spierings, G., 1993. Wet chemical etching of silicate glasses in hydrofluoric acid based solutions. J. Mater. Sci. 28, 6261–6273. https://doi.org/10.1007/BF01352182.

Sypabekova, M., Jolly, P., Estrela, P., Kanayeva, D., 2019a. Electrochemical aptasensor using optimized surface chemistry for the detection of Mycobacterium tuberculosis secreted protein MPT64 in human serum. Biosens. Bioelectron. 123 https://doi.org/10.1016/j.bios.2018.07.053.

Sypabekova, M., Korganbayev, S., Blanc, W., Ayupova, T., Bekmurzayeva, A., Shaimerdenova, M., Dukenbayev, K., Molardi, C., Tosi, D., 2018. Fiber optic refractive index sensors through spectral detection of Rayleigh backscattering in a chemically etched MgO-based nanoparticle-doped fiber. Opt. Lett. 43, 5945–5948. https://doi.org/10.1364/OL.43.005945.

Sypabekova, Marzhan, Korganbayev, S., González-Vila, Á., Caucheteur, C., Shaimerdenova, M., Ayupova, T., Bekmurzayeva, A., Vangelista, L., Tosi, D., 2019b. Functionalized etched tilted fiber Bragg grating aptasensor for label-free protein detection. Biosens. Bioelectron. https://doi.org/10.1016/j.bios.2019.111765.

Yin, M.-J., Gu, B., An, Q.-F., Yang, C., Guan, Y.L., Yong, K.-T., 2018. Recent development of fiber-optic chemical sensors and biosensors: mechanisms, materials, micro/nano-fabrications and applications. Coord. Chem. Rev. 376, 348–392. https://doi.org/10.1016/j.ccr.2018.08.001.